Lasers in Manufacturing Conference 2017

Investigation of selective laser melting spatter characteristics for single- and multi-beam strategies using high speed imaging

Thorsten Heeling[a,*], Marcel Gerstgrasser[a], Konrad Wegener[a]

[a]*Institute of Machine Tools and Manufacturing, ETH Zurich, 8092 Zurich, Switzerland*

Abstract

Selective laser melting is one of the most promising technologies for the additive manufacturing of near-fully dense metal parts of very high complexity. Since the process still needs improvement in terms of repeatability, robustness and quality an increasing number of possible strategies are proposed to do so. But because of the high speed and small scale of the melt pool the process dynamics are mainly known from simulation models that neglect stochastic phenomena, so that improvements are discussed based on an idealized understanding. Therefore this paper tries to make aware of the processes' randomness using high speed imaging, enabling a look into the dynamics of single-beam as well as innovative multi-beam processing of stainless steel 316L. A focus is placed onto the difference in spatter characteristics because the spatter leads to random errors within the parts that are unpreventable to a certain extent but are directly influencing the resulting part's quality.

Keywords: Spatter Characteristics; Multi-beam Strategies; High Speed Imaging; Selective Laser Melting; Additive Manufacturing

1. Introduction

As a metal additive manufacturing process selective laser melting is offering the possibility to manufacture metal parts of high geometric complexity without part specific tools. In a first step a thin layer of metal powder is deposited onto a build plate. In the second step the parts' cross sections are irradiated by a laser beam so that the powder as well as previous layers and tracks are molten and solidified to result in a near-fully dense part after a high number of single layers. Certainly, there are still a couple of problems with laser-based additive manufacturing technologies such as residual stresses, pores, cracks and spatter. While

* Corresponding author. Tel.: +41 44 6 33 44 33
E-mail address: heeling@iwf.mavt.ethz.ch.

there is much research on the fields of stresses, pores and cracks, there is just little research on the field of spattering within the selective laser melting process.

According to Liu et al., 2015 two different types of spatter, droplet and powder spatter, exist which are a result of the recoil pressure. Using stainless steel 316L their study indicates an influence of the energy input on the spatter behavior, including spatter size, scattering state and jetting height. They find that the average spatter size is almost three times that one of the powder. For the metal powder CoCr, Wang et al., 2017 have also proven that the laser energy input indeed influences the spatter behavior. Higher inputs result in stronger spattering intensity, including the increase of droplet and powder spatter appearance. Those two spatter types scatter around and jet higher away from the melt pool. Beside stainless steel 316L, Simonelli et al., 2015 have also investigated the spatter behavior of the metal powder AlSi10Mg and Ti6Al4V. Irrespective of the used metal powder, the spherical melt pool spatter is much larger than the size of the original powder, as already mentioned above. In the studies of Anwar and Pham, 2016 and 2017 the spatter formation is investigated by varying the inert gas flow velocity, scan strategy and part placement for AlSi10Mg powder. A reduction of the gas velocity causes a higher spatter contamination of the powder bed. And regardless of the gas velocity, the scan in the direction of the flow induces more smoke and greater contamination to the process. Mumtaz and Hopkinson, 2010 investigated the influence of the pulse shape on the part's surface roughness as well as the spatter generation during build-up. Due to a gradual heating and a lower peak power, ramp up pulses were found to be beneficial to reduce the amount of spatter and the size of the plume. And Matthews et al., 2016 show a connection between the pressure within the build chamber and the spatter phenomena. While at ambient pressure the plume is directed mostly upwards, sucking gas from the sides of the melt pool into the plume, at low pressures the metal vapor is expanding equally to all sides. Therefore higher pressures force powder particles on the side of the melt pool to be sucked into the plume while at low pressure the particles are blown away from the melt pool up to an extent where no powder remains around the melt pool.

The above mentioned research covers the basics of the generation of spatter within the selective laser melting process. But the imaging that was used lacks a high amount of frames per second as well as a high resolution so that highly dynamic effects as well as fast spatter particles cannot be investigated. Also there is no real quantification of the spatter particles yet because a quantification that uses sieving cannot measure particles in the size of the powder particle size distribution. Furthermore the amount of tested parameter sets, that were tested yet, is quite small and often parameter sets are far from actual processing parameters. Therefore high speed imaging with 30'010 images per seconds and a resolution as high as 15 µm per pixel is used within this study to quantify the spatter characteristics using automatic image processing. This is used to not only investigate single-beam strategies but innovative multi-beam strategies as well.

2. Experimental

2.1. Setup

The high speed imaging of the selective laser melting process is done on a laboratory machine. The machine features two independent 200 W continuous wave fiber lasers with a wavelength of 1070 nm (IPG YLR-200-WC) and two independently controllable scan heads (SCANLAB hurrySCAN III 14) with f-theta optics. The positioning of the scan heads allows a scan field overlap of about 160 mm x 280 mm, on which both beams can be deflected independently or synchronized. In the center of this overlap a build plate of 100 mm diameter is positioned. For the high speed imaging a Phantom V12 camera is used, recording 30'010 frames per second of 512 x 256 pixels and a resolution of 15 µm per pixel. Due to the size and working distance of the camera and optics the machine has to be used with an opened front door. To guarantee a shielding gas

atmosphere, the irradiated area is continuously shielded by a concentrated stream of grade 4.5 nitrogen from the left of the chamber.

2.2. Elaborated scan strategies

Three different scan strategies are being investigated within this study. The first one is a common unidirectional single-beam strategy that one can find on any commercially available machine. The second one is a multi-beam strategy for which both laser beams scan the same line with a defined offset in scan direction, either postheating or preheating the material, further on called offset strategy. The third strategy is a multi-beam strategy for which the second beam circularly moves around the first beam (further on called wobbling strategy), so that a wider area around the melt pool is heated and/or molten. The strategies are illustrated in Fig. 1. The multi-beam strategies are aiming to a reduction of distortion due to the reduction of temperature gradients and cooling speeds. These effects are being investigated at another point.

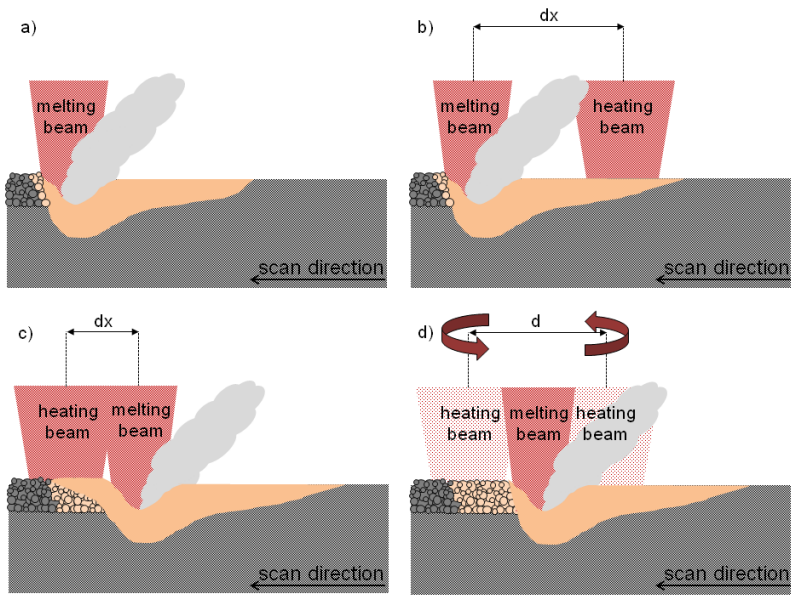

Fig. 1. Illustration of the elaborated single- and multi-beam strategies. a) single-beam, b) multi-beam postheating, c) multi-beam preheating and d) multi- beam wobbling strategy.

2.3. Experimental design

Prior to the high speed imaging twenty layers are deposited and solidified to guarantee a stabilized powder layer comparable to the actual process. The irradiated sample areas for imaging are 5 mm x 5 mm in size to enable a view into start and end of every line. The lines are scanned parallel to the x-axis of the camera so that a single line does not move perpendicular to the focal plane of the optics. To allow the synchronized multi-beam strategies to work as intended the scan fields are calibrated prior to the process as described in Heeling et al., 2016.

The investigated parameter sets are aiming to get an insight into the influence of the general scan speed, the influence of the beam offset within the multi-beam offset strategies (preheating and postheating) at two different scan speeds as well as a first look into the multi-beam wobbling strategy as a completely new strategy. The parameter sets are listed in Table 1. Powder material of stainless steel 316L is used for all experiments. The melting beam (1) spot diameter is set to 90 µm and the heating beam's (2) to 270 µm. The melting beam power is set to 200 W and the hatch distance to 82.5 µm for all parameter sets.

Table 1. Overview of elaborated strategies and process parameter sets.

Strategy	Scan speed [mm/s]	Power 2 [W]	Beam offset [µm]	Wob. diameter [µm]	Wob. frequency [µm]
Single-beam	677, 833, 1000, 1250, 1500	0	0	0	0
Preheating	1000, 1500	100	-270, -180, -90, -45	0	0
Postheating	1000, 1500	100	45, 90, 180, 270, 360, 450, 900	0	0
Wobbling	1000	100, 200	45	500, 750	250, 375

3. Image Processing

The image processing is realized using a self-developed Matlab tool that optimizes the image's grayscales, identifies significant points within the images, associates points of different pictures to one another and tracks the movement of associated points over a sequence of images so that speeds can be calculated.

3.1. Image preparation

A preparation of the images prior to the processing is recommend to increase the amount of identified characteristic points. The higher the grayscale gradients, the more characteristic points will be identified by the algorithm. While some spatter particles are bright enough to be identified easily, those which are smaller, faster or just colder are darker and will less likely be identified. Therefore the grayscale within a range is boosted to a higher value, as depicted in Fig. 2, so that the grayscale gradients are high enough to detect these originally darker particles. Grayscale values lower than a certain threshold are set to zero to reduce the noise.

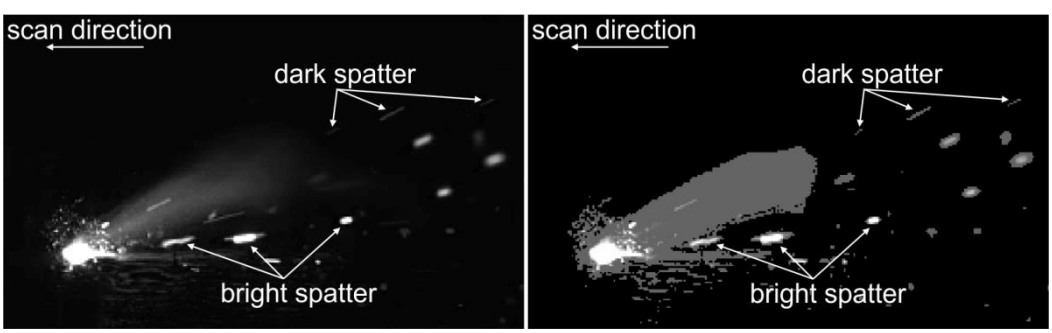

Fig. 2. Raw image (left) and image with adjusted grayscale values (right). Examples for bright and dark spatter particles are given.

3.2. Identification and filtering of characteristic points

The characteristic points and circles for the tracking of the laser spot are identified using Matlab internal functions. The tracking of the laser spot is necessary because of the plume in which characteristic points are identified due to the grayscale gradient. Therefore the area around the laser spot needs to be excluded from further processing to reduce the error. The result of identifying and filtering the characteristic points is illustrated in Fig. 3.

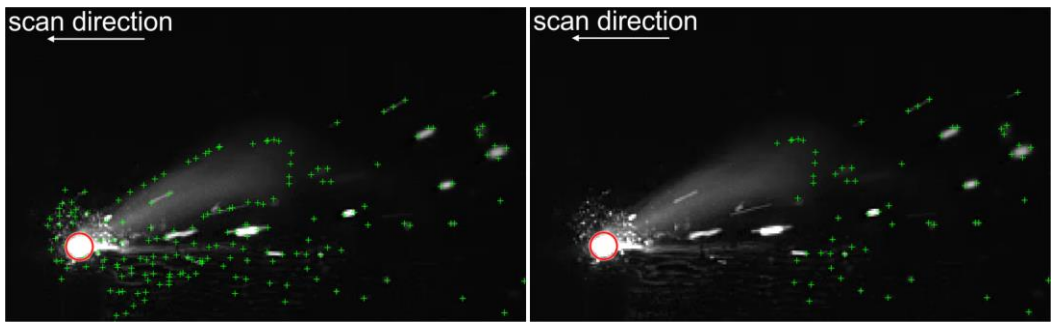

Fig. 3. Unfiltered (left) and filtered (right) image with identified points on spatter particles (green crosses) and the identified laser spot position (red circle).

3.3. Tracking of associated points

At this point still a large amount of characteristic points is stored for every single image. Some of those are wrongly identified and there are multiple characteristic points on any spatter particle. But the goal is to achieve a data set in which just a single point per spatter particle is tracked. Therefore the points on actual spatter particles need to be identified and associated over a sequence of images. This is done by calculating the distances between these points.

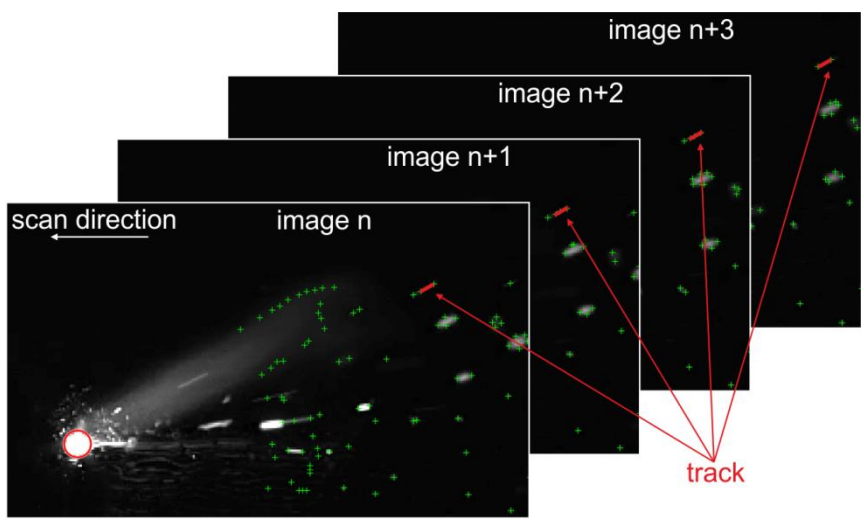

Fig. 4. Illustration of the process that tracks a spatter particle over a sequence of images.

Assuming that the distance between two points on a spatter particle with constant speed doesn't change much between two images, the distances of associated points can be identified in a sequence of images and therefore tracked over a limited time. Since a spatter particle can have several identified characteristic points, tracks that have the exact same point in common are reduced to a single track. This process is illustrated in Fig. 4. A hand count of three videos, each covering three scan lines, showed that this algorithm is able to identify about 75% of the spatter particles in average.

4. Results and Discussion

The strategies and parameter sets are characterized by the amount of spatter, the spatter velocity and brightness. While the spatter amount just gives an overall idea, velocity and brightness can be used to differentiate the spatter particles. While slower and larger ones tend to originate from the melt pool, darker and faster ones often originate from the surrounding powder material which is sucked into the plume and blown away. In the following a spatter particle is considered dark if the above mentioned grayscale increase was necessary. Examples of these two kinds of spatter particles are shown in Fig. 2. The spatter count is taken as the automatically identified amount of spatter per millimeter scan length. In general it can be observed that most of the spatter is blown to the back of the melt pool and therefore opposite to the scan direction. This opposes the findings of Liu et al., 2015 and Wang et al, 2017 who found a large portion of spatter being ejected mainly upwards. This might be because in these studies very low scan speeds were used that are far smaller than those commonly used for selective laser melting.

4.1. Single-beam strategy

The results of the single-beam experiments are shown in Fig. 5. The spatter count shows a clear trend of an increasing amount of spatter with increasing scan speed. The minimum is at 4.9 counts/mm for the minimum scan speed of 667 mm/s and the maximum is at 16.3 counts/mm for the maximum scan speed of 1500 mm/s. At 1000 mm/s a bump can be observed that disturbs the otherwise linear trend. While the amount of dark spatter follows this trend, the amount of bright spatter is just increasing linearly. Also the amount of dark spatter is far larger than the one of bright spatter particles.

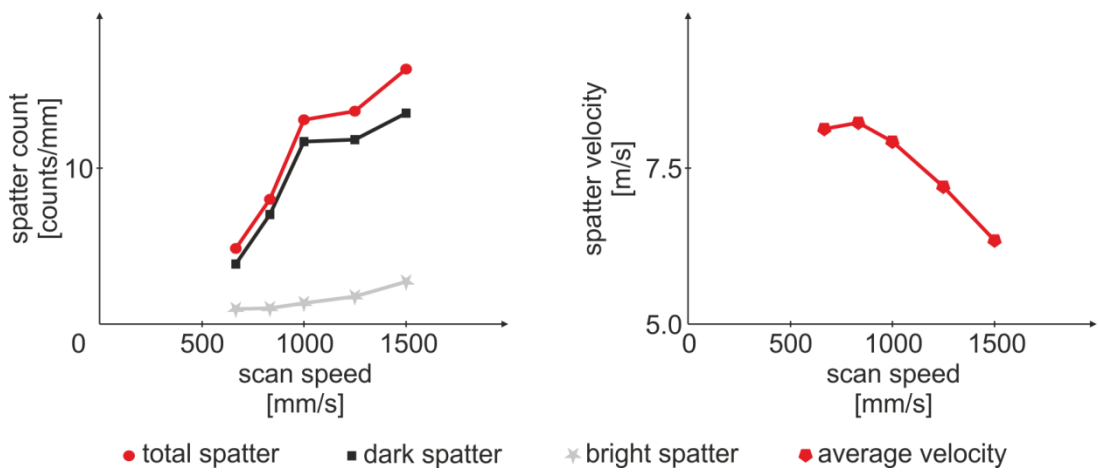

Fig. 5. Spatter data for single-beam experiments taken from the automatic processing of the high speed images

The increase in bright spatter can easily be connected to the reduction of the energy density with increasing scan speeds. The smaller energy density results in smaller, less deep melt pools and thus a worse wetting of the melt pool to the previous layer and track. Because of the weaker wetting to the surrounding the probability for melt to exit the melt pool due to high melt pool velocities and evaporation is higher. To explain the strong increase of dark spatter, meaning mainly powder material that is blown away, two effects have to be considered. The first one is connected to the scan speed as well as the size of the melt pool. At slower scan speeds the melt pool front is wider and most of the laser power is absorbed within the melt pool. Therefore surrounding powder particles can be caught by and included into the melt pool due the melt's convection before being irradiated by the laser. At higher scan speeds, the part of the laser beam that is absorbed within the powder increases and it is more likely that powder is moved upwards by air streams that evolve due to evaporation and heated gas. But this movement is comparably small and not strong enough to let the powder material be considered as spatter. At this point a second effect, the plume, comes into play which sucks the moving particles in and accelerates them to the back of the melt pool. Considering that the plume is the result of evaporation at the melt pool front it could be expected that the effect should increase with lower scan speeds that result in higher energy densities and more evaporation. Though, the spatter counts show an antithetic trend. The high speed images offer a possible explanation. While at high energy densities the plume is stable and strongly directed to the back of the melt pool, the plume of lower energy densities is fluctuating and moving around, covering and therefore affecting a far larger area of powder material. The strength of the backward gas stream induced by the plume is reflected by the particle velocities. With decreasing strength and with increasing fluctuation the acceleration of the particles decreases. Thus the average particle velocity decreases with increasing scan speed. The maximum spatter velocity value is about 13 m/s.

4.2. Multi-beam strategies

The spatter data of the preheating and postheating multi-beam strategies is depicted in Fig. 6. Compared to the spatter count of the single-beam strategy the minimum count of the offset strategies is slightly lower for equal scan speeds as well as equal energy densities. The spatter count of the offset strategy shows an increasing trend from the preheating parameters to postheating with an offset of 360 µm. Within the preheating parameter sets the increase is comparably low, while the spatter count increases significantly with increasing postheating offsets. The grayscale values of the spatter show that the ratio of dark to bright spatter particles decreases with increasing postheating offsets, meaning that the increase of bright spatter is stronger than the one of dark spatter.

The low amount of spatter within the preheating parameter sets can be explained by the heating beam melting small particles which are then agglomerating to larger melt droplets. Due to the higher mass of the droplets compared to the previously small powder particles and wetting to neighboring particles, the chance of being sucked into the plume is reduced. With higher preheating offsets the time from heating to melting beam is larger so that more particles can be molten and agglomerated before the plume reaches these particles. Therefore a higher offset reduces the amount of spatter in case of preheating strategies. But in case of postheating strategies a high offset has a bad influence on the spatter characteristics. The high speed images show that for offsets larger than 90 µm the second beam disintegrates large melt pool spatter particles into several smaller ones and rapidly heats dark spatter particles that are blown to the back of the melt pool. Furthermore particles are heated by the larger heating beam that the melting beam did not reach, leading to movement on the powder side that increases the likeliness on getting influenced by the plume. All of these effects lead to a significant increase in the amount of bright spatter for higher postheating offsets. The maximum is reached at 360 µm and the chance of melt pool spatter being disintegrated by the second

beam reduces afterwards due to the opening angle of the spatter cone. The trends and effects are the same for the scan speeds of 1000 mm/s and 1500 mm/s. But the 1500 mm/s spatter count experiences a currently not explainable drop at a postheating offset of 270 µm. As for single-beam strategies the spatter count is higher for faster scan speeds due to less deep melt pools and worse wetting to the surrounding.

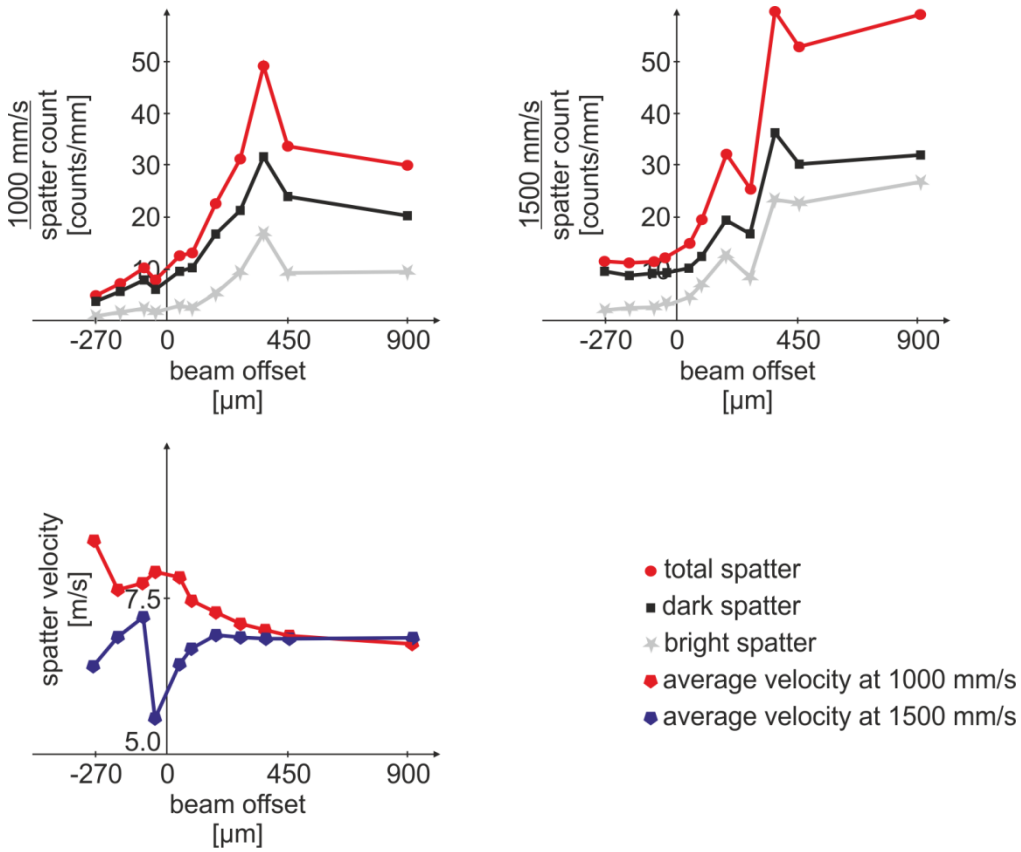

Fig. 6. Spatter data of the offset multi-beam strategies for preheating offsets (negative values) and postheating offsets (positive values) for two different scan speeds.

In case of the wobbling strategies the same effects result in the data listed in Table 2. Due to the higher speed of the heating beam which is circulating around the melting beam, the interaction time with the powder particles is reduced. This allows very small particles to be molten and agglomerated while the movement within the powder is kept at a minimum. Therefore less powder particles are sucked into the plume. The brightness of the spatter particles supports this assumption since the ratio of dark to bright spatter particles is even smaller than for large preheating offsets. For higher powers the spatter count increases caused by an increasing amount of melting and evaporation within the powder layer.

The spatter velocities of the multi-beam strategies are less helpful to explain the actual spatter behavior. As for the single-beam strategies the velocities are lower for higher scan speeds, presumably due to a less powerful plume. But for high postheating offsets of both scan speeds as well as the wobbling strategies the average spatter velocities converges to 7 m/s. As for single-beam strategies the maximum spatter velocity of the investigated multi-beam strategies is about 13 m/s.

Table 2. Spatter data of the wobbling parameter sets

Power 2 [W]	Wob. diameter [µm]	Wob. frequency [µm]	Total spatter count [counts/mm]	Dark spatter count [counts/mm]	Bright spatter count [counts/mm]
100	500	250	7.13	5.38	1.69
200	500	250	21.93	11.62	10.16
100	750	375	10.56	6.98	3.49
200	750	375	16.42	10.93	5.47

4.3. Influence of spatter on part quality

While a minimum of spatter particles should be aimed for to optimize the process, the influence of the spatter particles is not equally bad. Small, dark particles which are originating from the neighboring powder layer and which are blown away by the plume are just slightly reducing the amount of powder that is molten within the next tracks. Since the blown powder particles that drop down on another part are not larger than other powder particles within the powder bed, there is no significant influence on the quality of those parts. Small powder particles that are rapidly heated by passing the laser within the plume as well do not influence surrounding parts. But the shadowing of the current melt pool might induce errors to the current track. The largest threat to the part quality lies within large melt pool spatter since these are far larger than common powder particles. If a large spatter particles drops down on a cross section which is yet to be molten, the necessary amount of energy to get a sufficient wetting to the previous layer is far larger. Therefore large spatter particles significantly increase the risk for pores within the parts and need to be avoided. Taking this into account even the higher spatter count of the postheating strategies might be acceptable as long as large particles are disintegrated into ones of the size of the common powder particles by the second beam.

5. Conclusion

The presented evaluation of high speed images shows that there are different kinds of spatter and different effects that result in spattering within the selective laser melting process. And a second beam used for heating or melting within the vicinity of the melt pool has a significant effect on the spatter phenomena.

In general two kinds of spatter have to be distinguished. First, spatter particles that are originating from the melt pool which are characterized by a large size, high temperature and therefore a high brightness but a comparably low speed of about 4 to 7 m/s. Second, spatter particles that are originating from the powder layer and are blown away due to the influence of the plume above the melt pool. These are characterized by a small size and velocities as high as 13 m/s. Depending on the fluctuation of the plume and the path of the powder particles within the plume the particles either leave the plume cold or rapidly heated within the laser beam. While the latter kind of spatter is less significant for the part's quality, a reduction of these spatter particles is still recommendable. The large melt pool spatter particles on the other hand should be avoided to reduce the risk of pores within surrounding areas.

The comparison between single- and multi-beam strategies shows that within unidirectional single-beam scanning the scan speed is strongly influencing the amount of spatter. At low scan speeds deep melt pools are generated and a good wetting of the melt to the surrounding is achieved so that the chance for melt pool spatter is comparably low. Furthermore, a strongly directed plasma plume reduces the risk for surrounding powder particles of being blown away. Within the offset strategies the offset as well influences the spatter characteristics significantly. While for preheating the heating beam reduces the amount of spatter due to a prior agglomeration of small powder particles so that these are less likely blown away, at postheating the

heating beam might disintegrate large particles into several smaller ones and therefore increasing the spatter count. The wobbling strategy enlarges the benefit of the preheating to a wider area due to its circular movement around the melt pool.

Acknowledgement

The first author gratefully acknowledges the financial support of the Bosch Research Foundation (Bosch-Forschungsstiftung).

References

Anwar, A.B., Pham, Q.-C., 2016. Effect Of Inert Gas Flow Velocity And Unidirectional Scanning On The Formation And Accumulation Of Spattered Powder During Selective Laser Melting, Proc. of the 2nd Conf. on Progress in Additive Manufacturing, pp. 531-536.

Anwar, A.B., Pham, Q.-C., 2017. Selective laser melting of AlSi10Mg: Effects of scan direction, part placement and inert gas flow velocity on tensile strength, Journal of Materials Processing Technology 240, pp. 388-396.

Heeling, T., Zimmermann, L., Wegener, K., 2016. Multi-Beam Strategies for the Optimization of the Selective Laser Melting Process, Proceedings of the Annual International Solid Freeform Fabrication Symposium, Austin, TX, USA, pp. 1428-1438.

Liu, Y., Yang, Y., Mai, S., Wang, D., Song, C., 2015. Investigation into spatter behavior during selective laser melting of AISI 316L stainless steel powder. Materials and Design 87, pp. 797-806.

Matthews, M.J., Guss, G., Khairallah, S.A., Rubenchick, A.M., Depond, P.J., King, W.E., 2016. Denudation of metal powder layers in laser powder bed fusion processes, Acta Materiaia 114, pp. 33-42.

Mumtaz, K.A., Hopkinson, N., 2010. Selective laser Melting of thin wall parts using pulse shaping, Journal of Materials Processing Technology 210, pp. 279-287.

Simonelli, M., Tuck, C., Aboulkhair, N.T., Maskery, I., Ashcroft, I., Wildman, R.D., Hague, R., 2015. A study on the laser spatter and the oxidation reactions during selective laser melting of 316L stainless steel, Al-Si10-Mg and Ti-6Al-4V, Metallurgical and Materials Transactions A 46, pp. 3842-3851.

Wang, D., Wu, S., Fu, F., Mai, S., Yang, Y., Liu, Y., Song, C., 2017. Mechanisms and characteristics of spatter generation in SLM processing and its effect on the properties. Materials and Design 117, pp. 121-130